

# Mechanical model for the shear strength prediction of corrosion-damaged reinforced concrete slender and non slender beams

Antoni Cladera<sup>a,\*</sup>, Antonio Marí<sup>b</sup>, Carlos Ribas<sup>a</sup>

<sup>a</sup> Department of Industrial Engineering and Construction, Universitat de les Illes Balears, Ctra. Valldemossa km 7.5, 07014, Palma, Balearic Islands, Spain

<sup>b</sup> Department of Civil and Environmental Engineering, Universitat Politècnica de Catalunya-BarcelonaTech, Spain

## ARTICLE INFO

### Keyword:

Shear strength  
Reinforced concrete  
Stirrup  
Corrosion  
Deterioration  
Mechanical model  
Slender beams  
Short beams

## ABSTRACT

Steel corrosion in RC structures leads to a reduced reinforcement area, changes in steel mechanical properties, cracking and, eventually, concrete cover spalling, among other phenomena. Stirrups are generally small in diameter and, given their small concrete cover, they are more susceptible to corrosion than longitudinal reinforcement. Hence their corrosion significantly affects shear strength. Most existing models that deal with reduction in the shear strength of corrosion-damaged reinforced concrete (RC) structures are empirical; that is, they have been numerically fitted to test results. In this context, conceptual models based on structural mechanics principles and verified for corrosion-damaged members are still needed.

In this paper, the Compression Chord Capacity Model (CCCM), a shear mechanical model previously derived by the authors, is adapted to predict the shear strength of corrosion-damaged RC beams. For this purpose, the model parameters that can be affected by steel corrosion in RC beams were identified and modified accordingly. CCCM predictions were compared to the experimental results of 146 slender and non slender beams failing in shear, in which stirrups and/or longitudinal reinforcement was subjected to corrosion. The CCCM achieved very satisfactory shear strength predictions when reductions in reinforcement areas and web width were taken into account, with a mean value of the  $V_{test}/V_{pred}$  ratio equaling 1.19 and a 19.5% coefficient of variation. Finally, a parametric analysis was performed to show the predicted reductions in shear strength according to the CCCM compared to the experimental results of some especially relevant tests.

## 1. Introduction

Steel corrosion is one of the most frequent and relevant deterioration processes that reinforced concrete structures undergo. It causes reductions in reinforcement areas, changes in reinforcing bars' mechanical properties [1] and loss of bond properties between steel and concrete [2,3]. In addition, the volumetric expansion of corrosion products causes splitting stresses along corroded reinforcement, which lead to cracking and eventually to cover spalling. As reinforcement becomes more exposed, the corrosion rate may increase and the deterioration process might accelerate [4]. As a result of these phenomena, a reduction in stiffness, bond properties, anchorage capacity, flexural and shear strengths takes place that may affect their service performance and strength.

Although this corrosion phenomenon may seem a minor problem on the global agenda, current estimations indicate that the global cost of corrosion is the equivalent to 3–4% of the Gross Domestic Product of

industrialized countries; that is 1.45 trillion euros [5]. Moreover, as the first cause of climate change is increased CO<sub>2</sub> concentrations in the atmosphere, climate change may have a direct impact on the life span of concrete structures. A rising CO<sub>2</sub> concentration implies a higher carbonation rate and existing infrastructure's deterioration increases [6]. Moreover, rising average temperatures can also imply significant increases in the corrosion rates of reinforcements for not only the aforementioned carbonation case, but also for chloride corrosion [7]. As the direct and indirect costs of corrosion are immense, a slight acceleration in the corrosion process can mean a significant increase in global expenditure. Australian research [6] suggests that failure to take action in mitigating climate change could lead to more carbonation corrosion damage with rises of up to 400% by 2100 for temperate climate zones of Australia and a 15% increase in chloride corrosion damage. Other studies indicate a 115% increased risk of carbonation damage in the Carpathian region [8].

Most research into steel corrosion in concrete structures has focused on determining its causes, the mechanisms governing its evolution and

\* Corresponding author.

E-mail addresses: [antoni.cladera@uib.es](mailto:antoni.cladera@uib.es) (A. Cladera), [antonio.mari@upc.edu](mailto:antonio.mari@upc.edu) (A. Marí), [carlos.ribas@uib.es](mailto:carlos.ribas@uib.es) (C. Ribas).

<https://doi.org/10.1016/j.engstruct.2021.113163>

Received 4 March 2021; Received in revised form 18 August 2021; Accepted 5 September 2021

Available online 16 September 2021

0141-0296/© 2021 The Author(s).

Published by Elsevier Ltd.

This is an open access article under the CC BY-NC-ND license

(<http://creativecommons.org/licenses/by-nc-nd/4.0/>).

Nomenclature	
$a$	shear span measured between the support axis and the loading axis
$b_{eff,corr}$	effective web width after spalling
$b_w$	web width
$c_v$	concrete cover
$d$	effective cross-section depth
$d_0$	effective cross-section depth, $d$ , but not less than 100 mm
$f_{cm}$	mean concrete cylindrical (150 × 300 mm) compressive strength
$f_{ctm}$	mean concrete tensile strength considered in this paper to equal $0.30 \cdot f_{cm}^{2/3}$ in MPa, but not higher than 4.60 MPa
$f_{yw}$	mean shear reinforcement yield strength
$h$	cross-section depth
$m_0$	mass of a stirrup, link or steel bar before corrosion
$m$	mass of a stirrup, link or steel bar after corrosion
$n$	$E_s/E_c$ ratio
$s$	spacing of stirrups
$s_x$	spacing of vertical reinforcement ( $A_{swy}$ ) in a D-region
$s_y$	spacing of horizontal reinforcement ( $A_{swx}$ ) in the web in a D-region
$x$	neutral axis depth of the cracked section, obtained by assuming zero concrete tensile strength
$x_1$	neutral axis depth inside a D-region for non slender beams
$z$	inner lever arm. In the shear analysis of the reinforced concrete beams without axial force, the approximate $z \approx 0.9d$ value is normally used
$A_0$	cross-sectional area of steel before corrosion
$A_{min}$	cross-sectional area of steel after corrosion
$A_s$	cross-sectional area of longitudinal tensile reinforcement
$A_{sw}$	cross-sectional area of shear reinforcement
$A_{swx}$	cross-sectional area of the horizontal reinforcement placed in the web in a D-region
$A_{swy}$	cross-sectional area of vertical reinforcement in a D-region
$E_c$	secant modulus of elasticity of concrete, considered to equal $E_c = 22,000 (f_{cm}/10)^{0.3} \times 39$ GPa in this paper
$E_s$	modulus of elasticity of reinforcing steel, considered to equal 200,000 MPa
$K_{ad}$	factor taking into account the ratio between the shear strength of a non slender and a slender beam; Eq. (16).
$K_c$	factor equaling the relative neutral axis depth, $x/d$ , but not higher than 0.20; Eq. (6).
$V_{ctu}$	concrete contribution to shear strength; Eqs. (6) and (12)
$V_{ctu,min}$	minimum concrete contribution to shear strength; Eq. (6)
$V_{max}$	maximum shear force that can be sustained by the member, limited by crushing of struts; Eq. (8)
$V_{pred}$	predicted shear strength
$V_{su}$	shear reinforcement contribution to shear strength; Eqs. (7) and (13)
$V_{swx}$	contribution of horizontal web reinforcement to shear strength in a D-region; Eq. (15)
$V_{swy}$	contribution of vertical web reinforcement to shear strength in a D-region; Eq. (14)
$V_{test}$	measured shear strength during the test
$V_w$	shear force resisted along the critical shear crack
$\alpha_e$	modular ratio, $\alpha_e = E_s/E_c$
$\alpha_{cw}$	coefficient taking into account the state of stress in struts. See EC-2 [22] for further information
$\eta_{wt}$	weight loss ratio
$\eta_{sn}$	section loss ratio
$\eta_{l,sn}$	longitudinal reinforcement section loss ratio
$\eta_{w,sn}$	web reinforcement section loss ratio
$\nu_1$	strength reduction factor for concrete cracked in shear. See EC-2 [22] for further information
$\theta$	angle between the concrete compression strut and the beam axis perpendicular to shear force
$\varphi_0$	cross-sectional diameter of steel before corrosion
$\varphi_{min}$	cross-sectional diameter of steel after corrosion
$\Phi_{min}$	stirrup diameter
$\rho_l$	longitudinal tensile reinforcement ratio referring to effective depth $d$ and web width $b_w$ for beams with rectangular cross-section
$\rho_w$	transversal reinforcement ratio
$\rho_{sw}$	horizontal reinforcement ratio along the web
$\rho_w$	transversal reinforcement ratio
$\sigma_1, \sigma_2$	principal stresses in the concrete compressed chord
$\sigma_{swx}$	stress at the longitudinal web reinforcement in a D-region
$\sigma_{swy}$	stress at the vertical stirrups placed below the neutral axis in a D-region
$\xi$	size and slenderness effect factor, as given by Eq. (9)

the local effects on both steel properties and the interaction of reinforcement with the concrete surrounding it [9]. Despite their large number, fewer studies have aimed to study the effects of corrosion on a structure's overall behavior and safety [10–17]. By way of example, the effects of the above-mentioned corrosion, such as reduced reinforcement section areas due to reinforcement corrosion, not only brings about a reduction in the affected RC member's bending capacity, but also stiffness loss, which leads to stress redistributions toward less or non corroded areas, both longitudinally and transversely. Furthermore, reduction in steel ductility due to the corrosion effect can significantly affect the plastic redistribution ability of continuous structures, which is especially relevant in structures subjected to seismic action [13].

Another frequent situation is the change in failure mode that reinforcement corrosion may cause. Corrosion of longitudinal reinforcements obviously affects flexural strength more, but can also reduce shear or torsional strength. Indeed a reduction in reinforcement section or loss of bonding to concrete increases the width and depth of cracks and, therefore, reduces both the aggregate interlock and the contribution of the compression chord as its depth reduces. Besides, transverse reinforcement usually presents less concrete cover. Another interesting case is the effect of reinforcement corrosion in columns,

which can cause longitudinal reinforcement buckling by either stirrup rupture or merely by their sectional loss. Note that a change in failure mode can be accompanied by a structure's decrease in ductility.

It can be deduced from the above considerations that corrosion considerably affects the already complex resistant mechanisms of concrete structures by making the rigorous evaluation of the resistant capacity of structures with corrosion a difficult, but very important, task. Numerical methods are a necessary and very powerful tool to carry out this task [18–20] but, in general, the time and computational costs they require are still very high. In addition, there is still a way to go for their calibration to allow the objectivity of results [21] in very complex situations, such as brittle failure under shear stresses or adequately reproducing passive confinement effects.

However, in real engineering practice, the number of more aged and susceptible to corrosion structures grows, and it is necessary to have sufficiently precise tools, but at the same time easy to use, to be able to quickly evaluate its strength with reasonable safety, and check the need for performing a deeper analysis using numerical methods.

The models used in design do not seem the most suitable ones for evaluating existing damaged structures as they are often empirical in nature, and their equations have been derived from experimental results

from non corroded structures without being directly supported by theoretical models [22,23]. Therefore, correction coefficients must be used to correct the model's results, and be intended for intact structures that must also be empirically obtained [24]. Moreover, the safety criteria used in newly designed structures are of dubious application to structures with reinforcement corrosion, especially with structures whose resistance capacity has already been affected.

In this context, experimentally verified conceptual models based on principles of structural mechanics can play a fundamental role in the evaluation of corrosion-damaged structures because, in their derivation, the parameters governing behavior and structural resistance, and their influence, appear naturally. Therefore, they can be adapted to different situations by simply taking into account the differential aspects of the new situation without having to use correction coefficients. One different and acceptable issue is that some coefficients which define behavior can be calibrated with existing experimentation.

In order to assess the residual shear strength of corrosion-damaged concrete structures, several applicable conceptual or semi-empirical methods that have been experimentally verified with non deteriorated structures exist. These methods can be grouped into methods based on the contribution of the cracked web (aggregate interlock) as a major mechanism of resistance to shear [25,26], and those based mainly on the contribution of the uncracked compression chord in bending as a prime mechanism before collapse [27–31], among others. Of them all, the Multi-Action Shear Model (MASM [31]) and its natural evolution, the Compression Chord Capacity Model (CCCM [30]), have proven excellent versatility to be adapted and applied successfully to very diverse situations, and offer very good results for slender reinforced and prestressed concrete members with rectangular or T-cross sections [30], non slender beams [32], RC beams subjected to fatigue loads [33], steel fiber-reinforced concrete beams without stirrups [34], beams reinforced with fiber-reinforced polymers (FRP) bars [35] and beams externally strengthened on shear using shape memory alloys [36,37].

This paper addresses the shear strength of reinforced concrete structures affected by reinforcement corrosion using the CCCM, developed by the authors, by extending it to beams with corroded reinforcement. To do so, first the results of shear tests on structures affected by reinforcement corrosion and its effects on shear transfer actions were analyzed. Second, the model parameters that can be affected by corrosion were identified and their values modified accordingly. Finally, the model was verified with the results of 146 tests on beams with corroded reinforcement failing in shear, including slender and non slender beams.

## 2. Structural effects caused by the corrosion of the reinforcement

The structural effects caused by reinforcement corrosion are largely known. In 1997, Rodríguez et al. [38] concluded that reinforcement corrosion affected the performance of concrete beams by not only increasing both deflections and crack widths at the service load, and by also reducing the strength at the ultimate load. Moreover, reinforcement corrosion may modify the failure mode in concrete beams. In the experimental campaign involving 31 beams carried out in [38], while non deteriorated tested beams failed in bending, damaged beams mostly failed due to shear forces. Two effects were shown to be significantly relevant: reduction in the cross-section of reinforcement (especially due to pitting at stirrups) and concrete cover deterioration due to cracking and spalling. Finally, the researchers concluded that a conservative value of either the ultimate bending moment or shear strength could be predicted by using RC conventional models and considering the reduced section of both steel and concrete.

Coronelli and Gambarova [39] focused on the structural assessment of corroded reinforced concrete beams, and studied both the service and ultimate limit states. They highlighted that increasing corrosion levels tended to anticipate shear cracks, corrosion affected both a structure's strength and ductility at Ultimate Limit State (ULS), and that bond

conditions should be assessed and modeled to predict the structural element's ductility.

The degree of reinforcement corrosion is generally reported in papers as either the weight loss ratio or the cross-sectional loss ratio. The weight loss ratio,  $\eta_{wt}$ , can only be obtained by a destructive technique: a stirrup, link or any steel bar (or segment) is weighed before and after inducing corrosion:

$$\eta_{wt} = \frac{m_0 - m}{m_0} \times 100\% \quad (1)$$

where  $m_0$  is the mass of a stirrup, link or steel bar before corrosion and  $m$  is the mass after corrosion.

Although determining the weight loss ratio in the lab is easy, it is not a convenient factor for predicting shear strength. The cross-sectional loss ratio,  $\eta_{sn}$ , is a direct parameter for calculations and can be obtained as:

$$\eta_{sn} = \frac{A_0 - A_{min}}{A_0} \times 100\% = \frac{\varphi_0^2 - \varphi_{min}^2}{\varphi_0^2} \times 100\% \quad (2)$$

where  $A_0$  and  $\varphi_0$  are the cross-sectional area and diameter, respectively, of steel before corrosion;  $A_{min}$  and  $\varphi_{min}$  are the minimum cross-sectional area and diameter after corrosion. Note that  $\eta_{wt}$  is an indicator of the average degree of corrosion, meanwhile  $\eta_{sn}$  tries to indicate the maximum cross-section loss. Both indicators should be identical for completely homogeneous corrosion but, in general  $\eta_{wt}$  will be lower than  $\eta_{sn}$ . In Section 5.1 on the database used, the empirical correlation used to convert the reported weight loss ratios,  $\eta_{wt}$ , in cross-sectional loss ratios,  $\eta_{sn}$ , is explained.

Expansion of corrosion products from stirrups causes concrete cover spalling, which results in a decrease of the concrete section of the beam. Higgins et al. [40] observed that the amount of concrete damage depends primarily on stirrup spacing and cover distance (see Fig. 1), and they proposed Eqs. (3) and (4) based on empirical data and theoretical computations. Non overlapping spall damage comes into play for widely spaced stirrups, but as stirrup spacing tightens, the entire cover area may spall. Note that in the original publication [40], Eqs. (3) or (4) were used depending on stirrup spacing:  $s$ , was higher or lower than  $5.5c_v$ , but this term has been corrected in this publication (see the expressions on the right of Eqs. (3) and (4)) for presenting perfect continuity between both equations for this case:  $s = 5.5(c_v + \phi_v)$ .

$$b_{eff,corr} = b_w - 2(c_v + \phi_v) + \frac{s}{5.5} \quad \text{if } s \leq 5.5(c_v + \phi_v) \quad (3)$$

$$b_{eff,corr} = b_w - \frac{5.5}{s}(c_v + \phi_v)^2 \quad \text{if } s > 5.5(c_v + \phi_v) \quad (4)$$

where  $b_w$  is the original undamaged beam width,  $c_v$  is the concrete cover,  $\phi_v$  is the stirrup diameter and  $s$  is stirrup spacing.

Eqs. (3) and (4) become valid once significant corrosion induces cracks from on the concrete surface of beams. Higgins et al. [40] proposed using the previous equations when stirrups exhibit 10% average cross-section loss or based on field observations of concrete damage. For lower average cross-section loss, the partially damaged concrete cover may still contribute to shear strength. This simple approximation to take into account the reduction of the web width will be considered in this paper. However, other more refined procedure is proposed in [41] taking into account the amount of longitudinal compressive reinforcement and the attack penetration value.

Another very important structural effect caused by reinforcement corrosion is the change in bonding properties between concrete and steel. The loss of contact surface between the reinforcement and the surrounded concrete, due to corrosion and concrete splitting, produces a loss of bond strength and, eventually, may drive to shear failure due to loss of anchorage capacity. This effect can be accounted for by the CCCM, since it provides the position of the critical shear crack, which

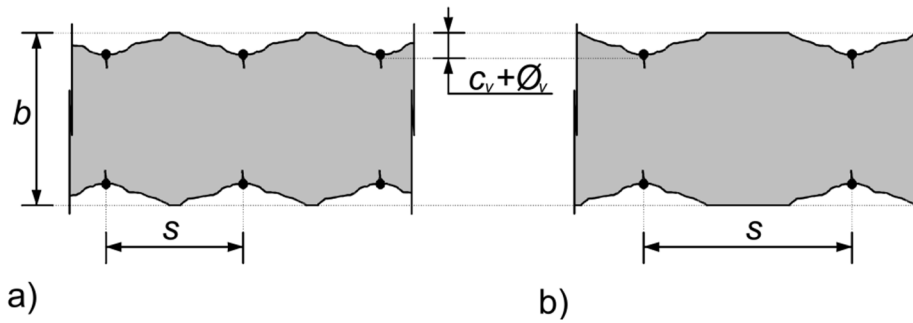


Fig. 1. Schematic plan view of concrete spalling in a beam web due to corrosion for two different stirrup spacings. Adapted from [40].

according to the model is given by the ratio between the cracking moment and the ultimate shear. However, the bond strength of the corroded bars is not given in the database used, so that this type of failure, is not being considered in the present paper. More information regarding bond properties of corroded reinforcing steel bar is found at [42].

### 3. The compression chord capacity model (CCCM)

The CCCM [30] is a shear design-oriented mechanical model based on a more complex analytical model referred to as the multi-action shear model (MASM) [31]. The MASM explicitly takes into account different commonly accepted shear transfer actions: shear transferred by the uncracked concrete chord, also called arching action; shear transferred across web cracks (through residual tensile stresses in the MASM); dowel action in longitudinal reinforcement if shear reinforcement is provided; tension in shear reinforcement if it exists; their interactions. Closed-form expressions have been obtained for the four shear transfer actions [31]. In the MASM, the critical shear crack is considered to initiate at a point where, upon failure, the bending moment equals the beam's flexural cracking moment. If no other premature failure takes place, shear strength is controlled by the flexural compression chord's capacity because it is the last element to initiate softening, which reduces its capacity as the crack propagates toward it inwardly. Failure is considered to occur when, at any point on the compression chord, the principal stresses reach Kupfer's biaxial failure envelope on the compression-tension branch [43]. The detailed derivation of the MASM is found in [31]. From a conceptual point of view, the model is fully compatible with a strut-and-tie model, even for beams without stirrups [44].

The use of four equations to obtain the shear strength is considered too complex for everyday calculations by practicing engineers, and the MASM was simplified to the CCCM [30,45]. The main premise of simplification was that, at failure initiation, both residual tensile stresses and dowel action were small compared to the shear resisted by the uncracked concrete chord and/or the contribution of shear reinforcement. In the next sections, CCCM equations are presented in detail for slender and non slender beams.

#### 3.1. Slender beams ( $a/d \geq 2.5$ )

The resulting expressions, particularized for RC members with rectangular cross-section, are summarized in Table 1 – Eqs. (5)–(11) and Fig. 2. Shear strength (Eq. (5)) is considered to equal the sum of concrete contribution,  $V_{cu}$ , and steel contribution,  $V_{su}$ , and has to be lower than the maximum shear strength given by strut crushing,  $V_{max}$ .

Concrete contribution is obtained by associating shear failure initiation with the stage represented by point A in Fig. 2b (adapted from [46]). This hypothesis substantially simplifies the problem with no significant loss of accuracy: the association allows the formulation of a failure criterion to be expressed in terms of the concrete stresses in the compression chord and as a function of the neutral axis depth,  $x$ , as seen

Table 1  
Summary of the CCCM equations for slender beams.

Equations	Expressions	
Shear strength	$V_R = V_{cu} + V_{su} \leq V_{max}$	(5)
Concrete contribution	$V_{cu} = 0.3\xi \frac{x}{d} f_{cm}^{2/3} b_w d \leq V_{cu,min} =$ $0.25 \left( \xi K_c + \frac{20}{d_0} \right) f_{cm}^{2/3} b_w d$	(6)
Shear reinforcement	$V_{su} = 1.4 \frac{A_{sw} f_y}{s} (d-x) \cot \theta$	(7)
Struts crushing	$V_{max} = \alpha_{cw} b_w z \nu_1 f_{cm} \frac{\cot \theta}{1 + \cot^2 \theta} \approx 0.225 f_{cm} b_w d$	(8)
Factors	Expressions	
Size and slenderness effects	$\xi = \frac{2}{\sqrt{1 + \frac{d_0}{200}}} \left( \frac{d}{a} \right)^{0.2} \leq 0.45$ d and $d_0$ in mm	(9)
Neutral axis depth	$\frac{x}{d} = \eta \rho_l \left( -1 + \sqrt{1 + \frac{2}{\eta \rho_l}} \right) \approx 0.75 (\eta \rho_l)^{1/3}$	(10)
Crack inclination	$\cot \theta = \frac{0.85d}{d-x} \leq 2.5$	(11)

in Eq. (6) to the left. A combined size and slenderness factor is defined by Eq. (9) and includes the size effect factor proposed by the ACI Committee 446[47] and recently adopted in ACI 318–19 Code [23]. Shear span,  $a$ , is the distance from the support to the resultant force of the loads producing shear on that support and its determination is direct for the beams subjected to point loads, like that included in the used database. For the beams with distributed loads, it can be computed as  $M_{u,max}/V_{u,max}$ , where  $M_{u,max}$  and  $V_{u,max}$  are the maximum absolute values of the internal forces in the region between the maximum bending moment and the zero bending moment where the considered section is located. For design purposes, in members subjected to a uniformly distributed load,  $a = 0.25L$  for simply supported beams and  $a = 0.5L$  for a cantilever beam.  $a = 0.2L$  for the positive (sagging) moment regions in continuous beams, and  $a = 0.15L$  for the negative (hogging) moment regions in continuous beams.  $L$  is the beam span or cantilever length. In order to develop a simpler code procedure, considering that the influence of shear span,  $a$ , is relatively small compared to the influence of other parameters, the term  $d/a$  could be substituted for a constant value [45]; e.g. 1/3.5, which represents a continuous beam with  $L/d$  equaling 17.5.

In some members, e.g. one-way slabs with low longitudinal reinforcement amount, the shear contribution due to residual stresses along the crack may be comparable to the contribution of the uncracked zone as  $x/d$  is small. For this situation, a minimum shear strength was proposed, which is the right-hand expression in Eq. (6), by explicitly taking into account the action of the residual tensile stresses in the web.

The stirrups' contribution is given by Eq. (7) for the particular case of vertical shear reinforcement, and is produced by the tensile stresses transmitted by stirrups in a length equaling  $0.85d$  (the horizontal projection of the first branch of the critical shear crack; see Fig. 2a and 2c). The term 1.4 comes from the mechanical derivation, see [30], and contemplates the confinement produced by the stirrups in the concrete compression chord.

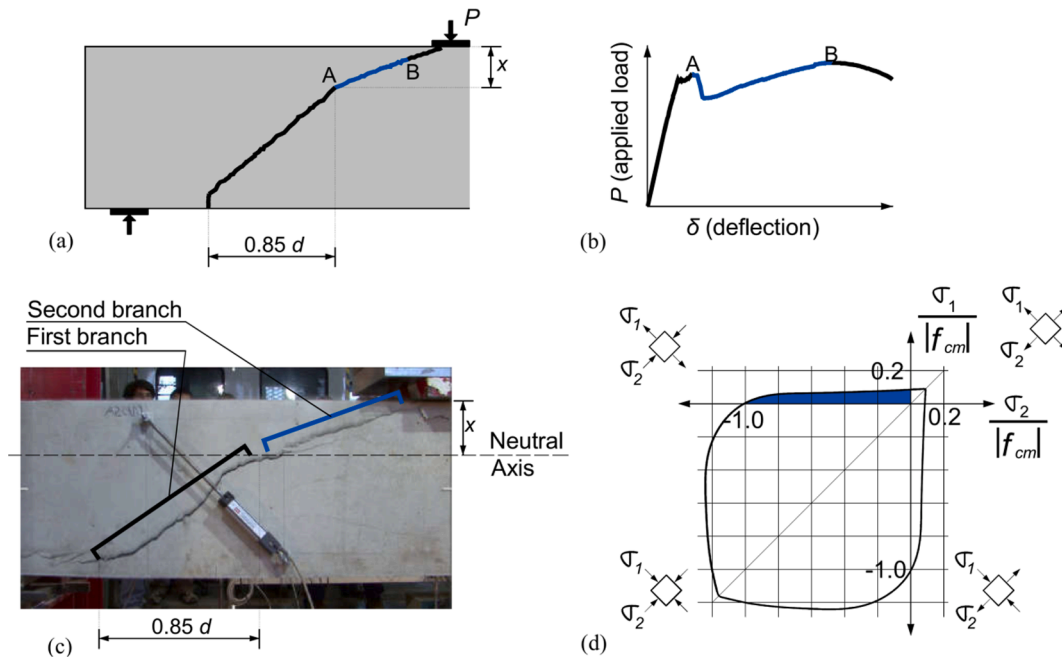


Fig. 2. Critical shear crack propagation: a) qualitative crack trajectory; b) schematic load–displacement curve; c) critical crack in a tested beam; d) adopted failure envelope for concrete under biaxial stress state.

The maximum shear strength is computed by a plasticity model (left-hand expression in Eq. (8)) by assuming for simplification reasons that the strut inclination equals the crack inclination (Eq. (11)). The expression on the right is a further simplification, achieved by introducing some typical values into the main equation, which also leads to very good results and makes use easier [45].

The predictions obtained by the CCCM have been compared in different papers to the experimental results obtained by hundreds of laboratory tests. For example, for the 784 RC slender beams without stirrups included in a previously published database [48], the obtained mean  $V_{test}/V_{pred}$  ratio value equaled 1.17, with 18.5% coefficient of variation. For the 170 RC slender beams with shear reinforcement that failed upon shear included in the database reported in [49], the mean  $V_{test}/V_{pred}$  ratio value equaled 1.16, with 14.1% coefficient of variation. These results are more accurate and precise than the predictions obtained with current code procedures [30,32,45].

### 3.2. Non slender beams ( $a/d < 2.5$ )

The shear strength of non slender beams is enhanced due to arching action. The CCCM was extended to include this case and for loads applied close to the support [32]. For this purpose, the differences in the structural behavior between slender and non slender beams were identified and incorporated into the original model formulation to adapt it to non slender beams. Table 2 (Eqs. (12)–(20)) summarizes the obtained expressions. In short, non slender beams show higher shear strength than slender beams and the following aspects of the structural response of non slender beams were taken into account [32]:

- Strain deformations are not planar and the neutral axis depth increases as the considered section approaches the support [50], i.e. as  $a/d$  decreases, see Fig. 3. This affects the concrete contribution to shear strength as it directly depends on the uncracked zone size. Eq (17) assumes a parabolic variation of  $x$  between  $a/d = 2.5$  ( $x_1 = x$ , B-region) and  $a/d = 0$  ( $x_1 = d$ ).
- Due to the distribution of stresses in the discontinuity region, a straight critical shear crack develops connecting the inner faces of

Table 2

Summary of the equations for non slender beams with rectangular cross-section.

Equations	Expressions
Concrete contribution	$V_{cu} = 0.3\xi\frac{x}{d}K_{ad}f_{cm}^{2/3}b_wd$ (12)
Web reinforcement	$V_{su} = V_{swy} + V_{swx}$ (13)
Vertical web reinforcement	$V_{swy} = \frac{A_{swy}}{s_x}(d-x_1)\cot\theta\sigma_{swy}$ (14)
Horizontal web reinforcement	$V_{swx} = 0.5\frac{A_{swx}}{s_y}(d-x_1)\tan\theta\sigma_{swx}$ (15)
<b>Factors</b>	
Non slenderness factor ( $a/d < 2.5$ )	$K_{ad} = 1 + (2.5 - \frac{a}{d})^2$ (16)
Neutral axis depth in D-region	$\frac{x_1}{d} = \frac{x}{d} + (1 - \frac{x}{d})(1 - 0.4\frac{a}{d})^2 \leq 1$ (17)
Crack inclination in D-region	$\cot\theta = \frac{a}{d} \geq 0.5$ (18)
Stress at vertical stirrups in D-regions	$\sigma_{swy} = \frac{f_{cm}K_{ad}}{\rho_l} \frac{x_1}{d} \cot^3\theta \leq f_{yw}$ (19)
Stress at longitudinal web reinf. in D-regions	$\sigma_{swx} = \frac{f_{cm}K_{ad}}{\rho_l} \frac{x_1}{d} \cot\theta \leq f_{yw}$ (20)

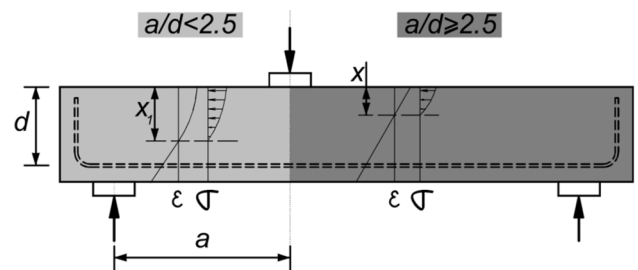


Fig. 3. Neutral axis depth ( $x$  and  $x_1$ ), stress and strain distributions, in slender and non slender shear spans.

the load to the support plates [51], see Fig. 4A. The inclination of this crack is given by  $\cot \theta$  in Eq. (18).

- When load is applied on the opposite side of the support reaction, see Fig. 4B, vertical compression stresses ( $\sigma_y$ ) are generated in the

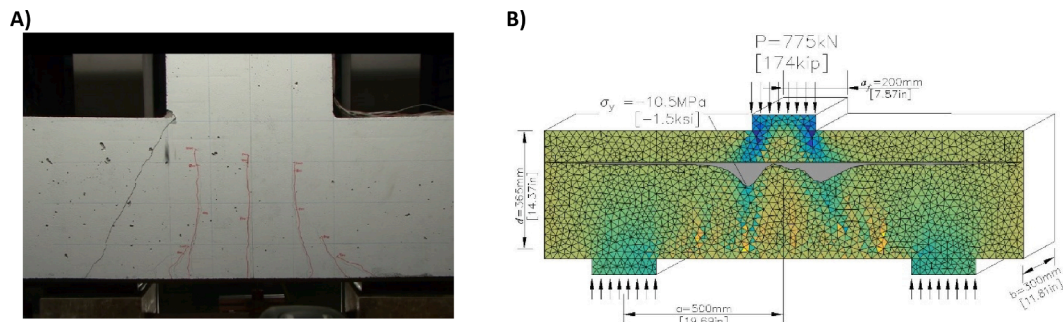


Fig. 4. A) Straight critical crack in beams subject to loads near supports. B) Vertical stresses generated in a short beam as observed in an NLFEA.

compression chord, which has a confining effect that may increase the shear stress  $\tau$  capacity of compression chord fibers.

By taking the above differences into account, a simple, but accurate equation, was obtained for concrete contribution to shear strength,  $V_{cu}$  in non slender beams.  $V_{cu}$  was obtained by multiplying the expression previously derived for slender beams by term  $K_{ad}$  (Eq. (16)) which, for  $a/d = 2.5$ , equals to 1 and, thus, results in shear strength equaling that of a slender beam.

Transverse reinforcement contribution,  $V_{swy}$  in Eq. (14), is smaller in non slender than in slender beams. The reasons for this reduction are: a) the increment in neutral axis depth reduces the number of transversal ties crossed by the critical shear crack in the tensile zone; b) the lower value of the stress in stirrups, which does not often yield at the crack. An equation to compute stress in the transversal reinforcement,  $\sigma_{swy}$ , and its contribution to shear resistance,  $V_{swy}$ , was also derived in [32], and is presented in Eq. (19).

Non slender beams are often reinforced with longitudinal web reinforcement. The contribution of this web reinforcement to shear strength,  $V_{swx}$ , was also incorporated into the CCCM extension. The term was mechanically derived and is usually much smaller than the shear carried by vertical web reinforcement; however, for low  $a/d$  ratios,  $V_{swx}$  may be equal, or be even higher, than  $V_{swy}$ .

A good agreement was observed between the proposed model's predictions and the experimental results compiled in two previously published databases [52,53]; e.g., for the 178 RC non slender beams with vertical web reinforcement, the obtained mean  $V_{test}/V_{pred}$  ratio value equaled 1.25, with 19.1% coefficient of variation. For the 86 RC non slender beams with vertical and horizontal web reinforcements, the mean  $V_{test}/V_{pred}$  ratio value was 1.28, with 22.3% coefficient of variation [32].

#### 4. Relevant aspects to consider when applying the CCCM to corrosion-damaged beams

Steel reinforcement corrosion may affect all the aforementioned transfer actions (shear transferred by the uncracked concrete chord, shear transferred across web cracks, dowel action in longitudinal reinforcement and the contribution of shear reinforcement) due to the loss of the sectional area of reinforcements, the reduction in web width owing to concrete cover spalling and, in some cases, the reduction of effective depth due to concrete spalling of the compression chord caused by corrosion of compressive longitudinal reinforcement and shear reinforcement.

The loss of longitudinal reinforcement section leads to an increase in its tension and decreases its stiffness. Consequently, on the one hand, the steel strain and width of the crack increases and, on the other hand, neutral axis depth lessens, as this depends on the amount of longitudinal reinforcement. Increasing crack width decreases the shear transferred in the web through an aggregate interlock and by residual tensile stresses across the crack. Reduced neutral axis depth decreases the contribution

of the compression chord. Lastly, the diminished longitudinal reinforcement area and cover spalling reduce dowel action.

Transverse reinforcement corrosion reduces its cross-section and, consequently, its capacity to transfer shear through the tensile stresses in this reinforcement, which affects the direct contribution of shear reinforcement to shear strength. In addition, as stirrups confine the concrete compression chord by enhancing its capacity to resist tangential stresses, loss of stirrups' cross-section also leads to a reduction in the confinement of the compression chord concrete.

In this work, the corrosion effects were taken into account in the CCCM as follows:

- (1) Regarding longitudinal reinforcement, to calculate the amount of longitudinal reinforcement,  $\rho_b$  and, consequently, the relative neutral axis depth,  $x/d$ , by means of Eq. (10), only the remaining area after loss due to corrosion was considered. With non slender beams, this reduced amount of longitudinal reinforcement was used for computing the effective stress at stirrups and web reinforcement (Eqs. (19) and (20)).
- (2) Corrosion products' expansion may create cracks in concrete and cause concrete spalling. As suggested by [40], web width  $b_w$  was substituted for  $b_{eff,corr}$  defined by Eqs. (3) and (4) when stirrups presented an average cross-section loss over 10%. For less damage, full web width  $b_w$  was used. The reduction in web width influenced determining the amount of longitudinal reinforcement,  $\rho_b$  and in the concrete contribution  $V_{cu}$  defined by Eq. (6) for slender beams and by Eq. (12) for non slender beams. The maximum strength of struts, Eq. (8), also depended on  $b_{eff,corr}$  in the event of an average cross-section loss exceeding 10%. In some cases, it might be necessary to also consider the reduction in overall beam height and, consequently, in effective depth  $d$  due to the concrete spalling of the compression chord owing to reinforcement corrosion. This reduction was not herein considered, but it can be easily taken into account from field observations in real cases or following the refined procedure given in [41].
- (3) The reduction in the cross-sectional area of web reinforcement was contemplated to apply the CCCM by considering only the remaining area when computing the stirrup contribution for slender beams (Eq. (7)), and the contributions of the vertical and horizontal web reinforcements (Eqs. (14) and (15)) for non slender beams.

## 5. Experimental verification

### 5.1. Database

A database including the results of 146 corrosion-damaged beams failing in shear was compiled, which comprised 84 non slender beams ( $a/d < 2.5$ ) and 62 slender beams ( $a/d \geq 2.5$ ). It was initially based on two previously published databases [54,55], but an effort was made to find new tests on slender beams to equilibrate the number of slender and

non slender beams. However, it was verified that most published results in the literature about the shear performance of reinforced concrete beams with corroded stirrups deal with non slender beams. The final database, presented as an appendix to this paper, includes the tests reported in [38,56–65] published between 1997 and 2019. Table 3 summarizes the range of the main variables in the database. All the beams had rectangular cross-sections. As the dimensions of most beams are small and not really representative of real civil engineering construction, fitting terms and coefficients to this database should be avoided, or the empirically derived methods could be unsafe for relatively big beams ( $h$  is lower than 610 mm for all beams in the database) or for beams with an ordinary amount of longitudinal reinforcement (minimum value of  $\rho_l$  for all beams in the database is equal to 0.99%).

Parameter  $f_{cm}$  in Table 3 refers to the cylindrical compression strength (samples of 150x300 mm). In some papers, cube strength (150x150 mm) is reported, in which case the value is converted as indicated in the Spanish Concrete Code [66] ( $f_{cm} = 0.90 \cdot f_{cm,cube}$ ). Moreover, the degree of corrosion of longitudinal or shear reinforcement is reported in the original papers as either the weight loss ratio,  $\eta_{wt}$  (Eq. (1)), or the cross-sectional loss ratio,  $\eta_{sn}$  (Eq. (2)). As the latter parameter allows the direct determination of a beam's strength reduction, the reported weight loss values should be converted into cross-section loss ratios. Lu et al. [54] proposed the procedure based on Eq. (21) to perform this conversion:

$$\eta_{sn}(\%) = \begin{cases} 1.3 + 0.987\eta_{wt}(\%) & \text{if } \eta_{wt} < 10\% \\ 6.1 + 0.939\eta_{wt}(\%) & \text{if } 10\% \leq \eta_{wt} < 20\% \\ 12.9 + 0.871\eta_{wt}(\%) & \text{if } 20\% \leq \eta_{wt} < 30\% \\ 19.9 + 0.801\eta_{wt}(\%) & \text{if } 30\% \leq \eta_{wt} \leq 40\% \end{cases} \quad (21)$$

Eq. (21) is represented in Fig. 5 (lines in blue). As can be seen, the equation does not present continuity at 10%, 20% and 30% and for  $\eta_{wt} = 0$ , it corresponds to  $\eta_{sn} = 1.3\%$ . For these reasons, Eq. (21) was simplified to Eq. (22), represented as a dashed red line in Fig. 5, which was used to convert the  $\eta_{wt}$  reported values into  $\eta_{sn}$ .

$$\eta_{sn}(\%) = 1.36\eta_{wt}(\%) \quad (22)$$

Eq. (22) will be used in this paper. However, it should be taken into account that depending on the type of attack (carbonation and/or chlorides) and the acceleration level of the corrosion procedure, the relationship between both indicators would change.

### 5.2. Comparison between the predicted and measured shear strengths

The main results of the comparison made of the predicted and measured shear strengths are presented in Table 4 and Fig. 6.

The CCCM performed satisfactory shear strength predictions when the reduction in the area of reinforcement (longitudinal and shear reinforcement) and of web width was taken into account. For the complete database, the mean ratio  $V_{test}/V_{pred}$  value equaled 1.19, with 19.95% coefficient of variation. The results for the slender and non slender beams were comparable (see Fig. 7). It must be highlighted that

**Table 3**  
Range of variables in the database.

	Non slender beams		Slender beams	
	Min	Max	Min	Max
# tests	84		62	
$b_w$ (mm)	120	254	120	200
$h$ (mm)	180	610	180	350
$f_{cm}$ (MPa)	21.0	50.0	22.5	50.0
$\rho_l$ (%)	0.99	2.30	1.77	3.27
$\rho_w$ (%)	0.14	0.90	0.10	0.52
$a/d$	1.00	2.20	2.50	4.70
$\eta_{l,sn}$ (%)	0	26.0	0	32.0
$\eta_{w,sn}$ (%)	0	68.4	0	97.2
$V_{test}$ (kN)	47.7	594	26.6	204

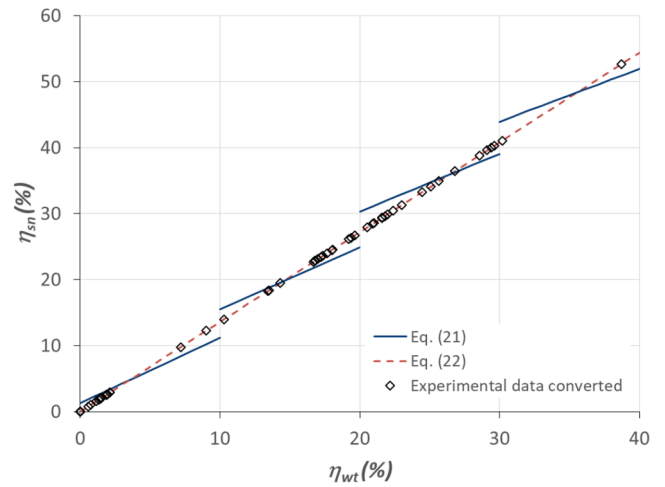


**Fig. 5.** Conversion from weight loss ratio,  $\eta_{wt}$ , to cross-sectional loss ratio,  $\eta_{sn}$ .

**Table 4**  
Comparison between the predicted shear strengths and the experimental results of the beams included in the database.

$V_{test}/V_{pred}$	All beams	Non slender beams	Slender beams
#	146	84	62
Mean	1.19	1.20	1.18
CoV (%)	19.95	17.50	23.06
Min	0.57	0.57	0.73
Max	1.94	1.57	1.94
5% percentile	0.80	0.80	0.81
95% percentile	1.54	1.49	1.67

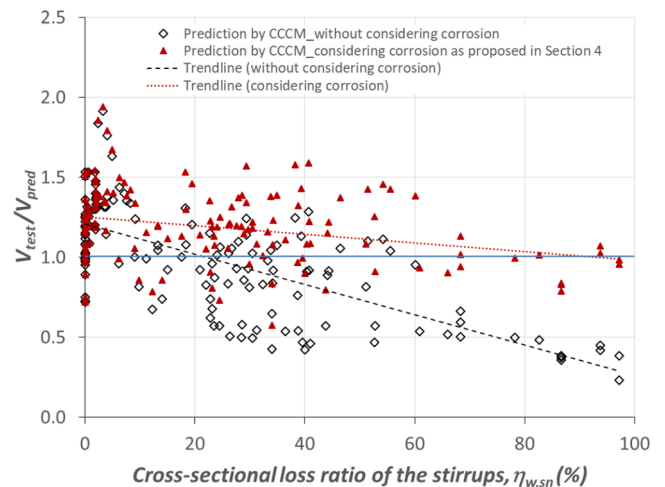


**Fig. 6.** Correlation of the experimental results and prediction versus the cross-sectional loss ratio of stirrups.

the safety levels (mean  $V_{test}/V_{pred}$  ratio value between 1.18 and 1.20) were similar to those obtained for undamaged concrete beams (between 1.16 and 1.25, see Section 3). The coefficient of variation of the entire database fell within the same range as for undamaged beams (between 14.1% and 22.3%; see Section 3), and was slightly higher only for the slender beams subset. The 5% percentile of the  $V_{test}/V_{pred}$  ratio is also similar for the two subsets of beams (0.80 vs. 0.81), although the minimum value of the  $V_{test}/V_{pred}$  is 0.57 for non slender beams, and 0.73 for slender beams. However, this low value belongs to test V3M-150 by [60], which failed for a lower shear force than other identical beams with higher reported damage level. In case of not considering V3M-150

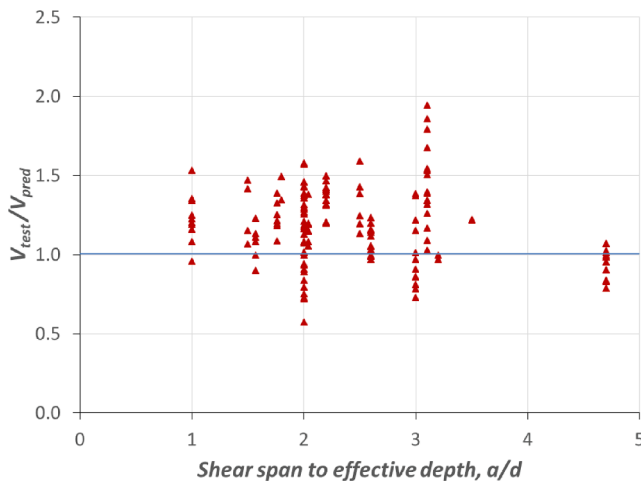


Fig. 7. Correlation of the  $V_{test}/V_{pred}$  ratio versus the shear span to effective depth ratio,  $a/d$ .

test, the minimum  $V_{test}/V_{pred}$  value would be 0.72 for the non slender beams, practically identical to 0.73 for slender beams. In any case, the results were deemed excellent when taking into account the high uncertainty level related to the damage determination for the steel and concrete cover of beams. In order to check how unsafe would be to use the CCCM without considering the corrosion effects, two calculations have been made with the model: 1) using the data of the intact (non-corroded) beams, and 2) using the data of the corroded beams, considering the area of the reinforcements measured after corrosion has taken place.

As can be seen in Fig. 6, the direct application of the CCCM would lead to very unconservative and dangerous results in the event of ignoring damage produced by corrosion (see the black rhombuses). However, when considering the cross-sectional loss ratio of stirrups and concrete cover deterioration, the CCCM was able to generally obtain safe results (the red triangles in Fig. 6), even for very high damage values for steel. For beams with low corrosion-damage (between 2 and 5%), predictions were more conservative. This could be related to the fact, as observed by different authors, that very low level damage (specially of longitudinal reinforcement) could enhance shear strength [62,67]. In any case, this effect should not be considered in a shear model given the high related uncertainty.

Concrete cover spalling is considered by the reduction in web width, as defined by Eqs. (3) and (4). As previously mentioned, when stirrups

exhibit an average cross-section loss over 10 %, the term  $b_w$  must be replaced with  $b_{eff,corr}$ . Fig. 8 shows the correlation of the experimental results and the CCCM predictions when considering, or not, this web width reduction. The red triangles denote that the average  $V_{test}/V_{pred}$  ratio is almost constant when contemplating web width reduction, as proposed in this paper. However, if the CCCM is applied only taking into account the cross-sectional reduction of steel, but not the reduction in web width due to concrete spalling (the black rhombuses in Fig. 8), the results tend to be unsafe for those cases in which significant spalling is envisaged according to Eqs. (3) and (4), i.e. low  $b_{eff,corr}/b_w$  values. The almost horizontal red trend line in Fig. 8 supports the good concrete spalling prediction carried out by Eqs. (3) and (4) from [40].

Finally, it must be emphasized that the procedure adopted herein was efficient in predicting the response of the simply supported RC beams tested in a lab, for which detailed data on the corrosion level and beam conditions are available. However, in the field, the key problem would probably be collecting reliable data on the corrosion level, as mentioned in [39].

### 5.3. Parametric analysis

In this section, the influence of steel corrosion on shear strength is studied in more detail by comparing the results obtained in some of the experimental campaigns included in the database with CCCM predictions. These tests were selected after taking into account that only one key parameter changed between different tests.

Fig. 9 compares the model's shear strength predictions for increasing values of the cross-sectional loss ratio of stirrups,  $\eta_{w,sn}$  with the experimental results obtained in four experimental campaigns [38,58,63,65]. Experimental strength upon failure is represented by red triangles, and predictions are given by a continuous blue line. The average values of the other involved parameters were considered and are represented in each graph. Note in Fig. 9a, 9c and 9d a trend change at  $\eta_{w,sn} = 10\%$ . This reduction in predicted shear strength is due to web width reduction according to Eqs. (3) and (4) [40].

In Fig. 9b, for  $\eta_{w,sn}$  values between 15% and 22%, the predicted shear strength remains constant: the failure predicted mode of these non slender beams for this corrosion level is due to the crushing of concrete struts (Eq. (8)), which does not depend on the amount of shear reinforcement. However for higher  $\eta_{w,sn}$  values, the cross-section reduction of stirrups changes the failure mode, and then strength reduces for increasing  $\eta_{w,sn}$  values.

Fig. 9d compares the predictions by CCCM with the tests results by Rodriguez et al. [38]. These beams were tested after suffering high corrosion levels at the reinforcement, including the longitudinal compressive reinforcement placed at the top of the beams. For this reason, the beams showed, during the tests, a reduction of the effective depth of the concrete section at the shear span, due to the spalling of the top concrete cover. This failure type is not clearly reported for the other beams included in the database and, as previously commented in Section 4, this effect is not considered in general in this paper for sake of simplicity. However, in Fig. 9d, two predictions by CCCM are shown: in blue without taking into account the reduction of the effective depth and in an orange dashed line, the predictions taking into account the spalling of the concrete cover above the stirrups, being safer the last predictions. In summary, for the 10 beams failing in shear from [38], the mean value of  $V_{test}/V_{pred}$  equaled 0.94 if the reduction is not taken into account, compared to 1.04 if the effective depth reduction is considered (in both cases the coefficient of variation is equal to 10.1%). This indicates that, as previously stated, it might be necessary in the cases with high amount of highly corroded compressive reinforcement to consider the reduction in overall beam height, according to the exposure of the concrete surfaces to aggressive agents.

Stirrups are smaller in diameter and more susceptible to corrosion given their smaller concrete cover compared to longitudinal reinforcement. For this reason, the main objective of the damaging procedure in

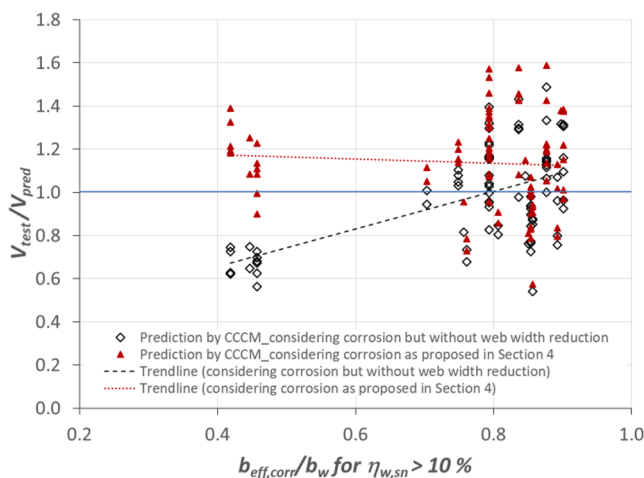


Fig. 8. Correlation of the experimental results and predictions versus the web width reduction ratio due to concrete cover spalling.

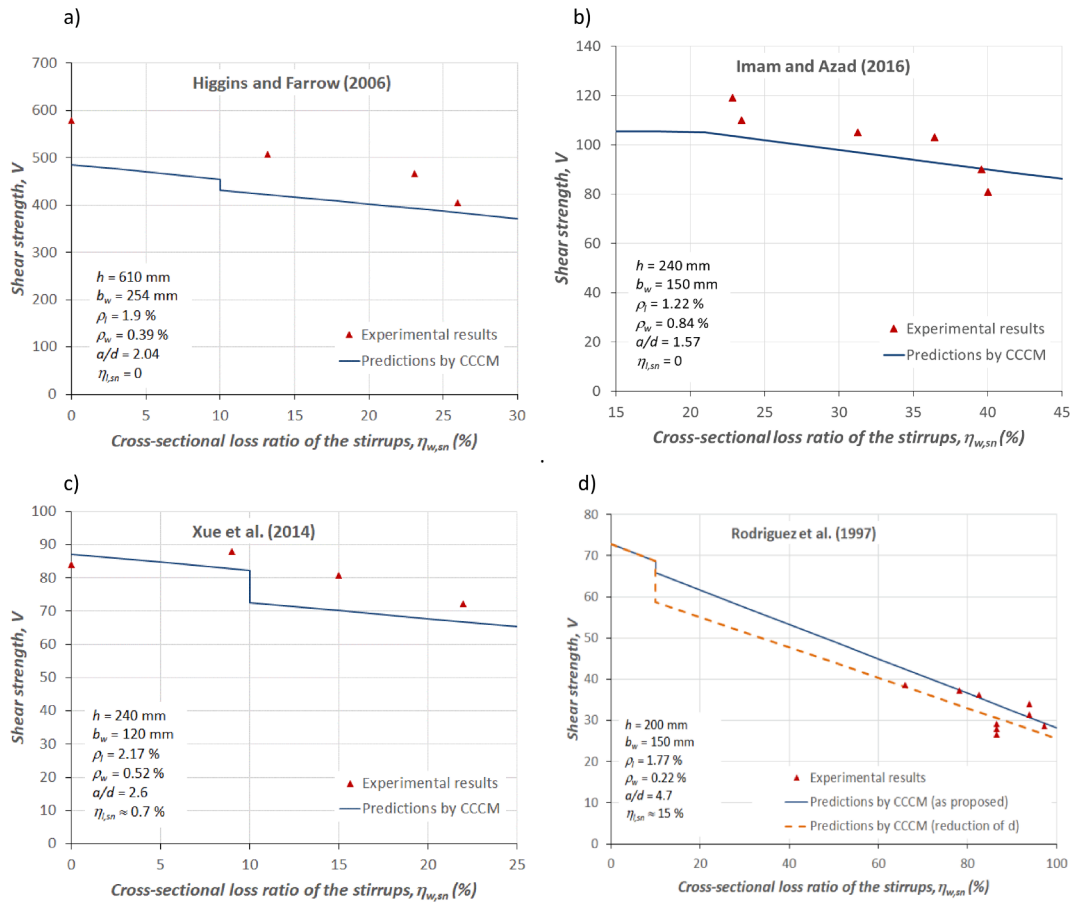


Fig. 9. Influence of the cross-sectional loss ratio of stirrups. a) non slender beams with slight loss; b) non slender beams with moderate loss; c) slender beams with slight loss; d) slender beams with high loss.

most published experimental campaigns has been to corrode shear reinforcement instead of longitudinal reinforcement. Consequently, there is not enough information to carry out a parametrical analysis based on existing empirical data to study the influence of the cross-sectional loss ratio of longitudinal reinforcement on shear strength because stirrups are more damaged than longitudinal bars in most cases. All in all, the CCCM predicts a decreased shear strength when the amount of longitudinal reinforcement lowers (see Fig. 10) as it brings about a reduction in the relative neutral axis depth,  $x/d$ , as previously mentioned. By considering all the beams included in the database with a cross-sectional loss ratio of longitudinal reinforcing bars over 1%, the

proposed procedure gave a good correlation with the experimental results (the red triangles in Fig. 10b). However, the CCCM would lead to unsafe results if applied without considering corrosion effects (the black rhombuses in Fig. 10b).

### 6. Conclusions

This paper focused on the shear strength of reinforced concrete beams affected by reinforcement corrosion, identifying the key parameters involved in shear strength that can be affected by corrosion. It also studied how these parameters influenced the predicted shear strength

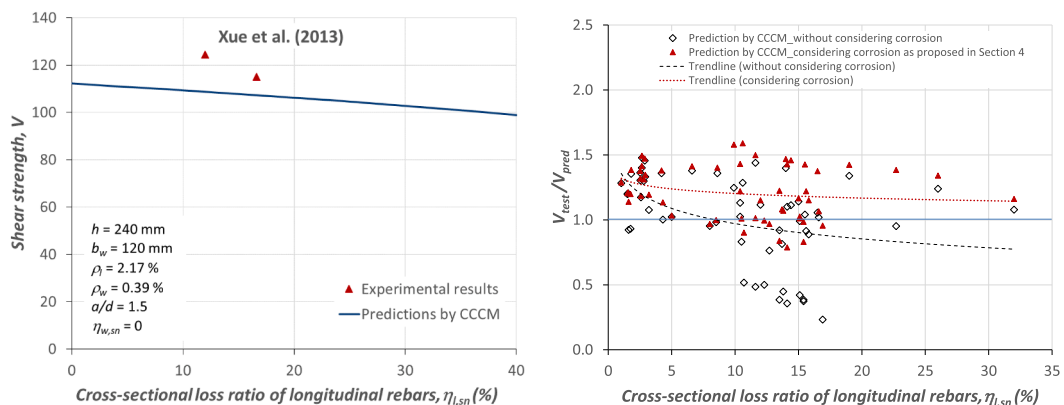


Fig. 10. Influence of the cross-sectional loss ratio of longitudinal reinforcing bars. a) comparison to two tested beams. b) the  $V_{test}/V_{pred}$  ratio for all the beams included in the database with  $\eta_{l,sn} > 1\%$ .

according to the Compression Chord Capacity Model (CCCM), previously developed by the authors. The following conclusions are drawn:

- The corrosion of stirrups and longitudinal reinforcement brings about a reduction in the reinforcement area and, eventually, concrete spalling, among other structural effects. Both effects must be taken into account to adequately predict the shear strength of corrosion-damaged beams.
- According to the test results, a reduction in the cross-sectional area of longitudinal reinforcement results in decreased shear strength. This result can be predicted by the CCCM as loss of longitudinal reinforcement reduces the relative neutral axis depth,  $x/d$  and, consequently, shear strength.
- The reduction in the cross-sectional area of web reinforcement reduces stirrup contribution to shear strength.
- The expansion of corrosion products may lead to cracks in the concrete cover, causing concrete spalling. The simple decreased concrete web width proposed by Higgins et al. [40], and presented in Eqs. (3) and (4), leads to very good results when combined with the CCCM. A more refined procedure, based on [41], could also be considered. The concrete spalling of the compression chord owing to reinforcement corrosion has not been generally taken into account in this paper, for simplicity reasons. However, it has been shown that in some cases it might be necessary to also consider it.
- The comparison of the shear strength predictions made by the CCCM and the experimental results of 146 beams included in a compiled

database shows a very good agreement, especially when considering that the database includes slender ( $a/d \geq 2.5$ ) and non slender ( $a/d < 2.5$ ) beams. For the complete database, the mean  $V_{test}/V_{pred}$  ratio value equals 1.19, with 19.95% coefficient of variation. The results for the slender and non slender beams are similar, and overall safety and scatter are comparable to those obtained by the CCCM for large databases of undamaged beams

- The parametric analysis shows the envisaged reductions in shear strength for the increasing cross-section loss ratio values of stirrups and longitudinal bars. These trends clearly agree with those observed with selected relevant tests, even for very severely damaged beams with cross-sectional losses exceeding 80%.

### Declaration of Competing Interest

The authors declare that they have no known competing financial interests or personal relationships that could have appeared to influence the work reported in this paper.

### Acknowledgments

The authors wish to acknowledge the financial support provided by the Spanish Ministry of Science, Innovation and Universities and European Funds for Regional Development (EU ERDF) through Research projects: RTI2018-099091-B-C22 (AEI/FEDER, UE) and RTI2018-097314-B-C21 (AEI/FEDER, UE).

## Appendix A

Reference	Specimen	$f_{cyl,150}$ (MPa)	$h$ (mm)	$b_w$ (mm)	$d$ (mm)	$\rho_l$ (%)	$\rho_v$ (%)	$f_y$ (MPa)	$f_{yv}$ (MPa)	$s$ (mm)	$a/d$	$\eta_{Lsn}$ (%)	$\eta_{w,sn}$ (%)	$V_{test}$ (kN)	$V_{pred, CCCM}$ (kN)	$V_{test}/V_{pred}$
Rodriguez et al. (1997) [38]	123	35.0	200	150	170	1.77	0.22	585	626	170	4.7	12.3	78.2	37.3	37.5	0.99 (1.10)*
	124	35.0	200	150	170	1.77	0.22	585	626	170	4.7	15.4	86.6	27.9	33.6	0.83 (0.92)*
	125	35.0	200	150	170	1.77	0.22	585	626	170	4.7	15.1	93.8	31.4	30.6	1.03 (1.13)*
	136	37.0	200	150	170	1.77	0.22	585	626	170	4.7	13.5	86.6	29.1	34.7	0.84 (0.93)*
	135	37.0	200	150	170	1.77	0.22	585	626	170	4.7	13.8	93.8	33.9	31.7	1.07 (1.18)*
	215	35.0	200	150	170	1.77	0.22	585	626	170	4.7	10.7	66.0	38.6	42.8	0.90 (1.00)*
	216	35.0	200	150	170	1.77	0.22	585	626	170	4.7	11.6	82.6	36.2	35.7	1.01 (1.12)*
	213	35.0	200	150	170	1.77	0.22	585	626	170	4.7	14.1	86.6	26.6	33.8	0.79 (0.87)*
	214	35.0	200	150	170	1.77	0.22	585	626	170	4.7	15.4	97.2	28.7	29.2	0.98 (1.09)*
	315	37.0	200	150	170	1.77	0.45	585	626	85	4.7	16.9	97.2	27.7	29.0	0.96 (1.16)*
Xu and Niu (2004) [56]	A	30.6	200	120	167	1.92	0.32	416	275	150	2	0.0	0.0	73.0	57.5	1.27
	B	29.7	200	120	167	1.92	0.32	416	275	150	2	0.0	0.0	71.4	56.9	1.26
	C	28.4	200	120	167	1.92	0.32	416	275	150	1	0.0	0.0	137.7	112.4	1.23
	A1	30.6	200	120	167	1.92	0.32	416	275	150	1	0.0	29.9 <sup>+</sup>	95.0	99.3	0.96
	B1	29.7	200	120	167	1.92	0.32	416	275	150	1	0.0	40.3 <sup>+</sup>	105.0	97.1	1.08
	C1	28.4	200	120	167	1.92	0.32	416	275	150	1	0.0	33.3 <sup>+</sup>	110.0	95.0	1.16
	A2	30.6	200	120	167	1.92	0.32	416	275	150	2	0.0	29.6 <sup>+</sup>	53.5	45.6	1.17
	B2	29.7	200	120	167	1.92	0.32	416	275	150	2	0.0	26.7 <sup>+</sup>	60.0	45.6	1.32
	C2	28.4	200	120	167	1.92	0.32	416	275	150	2	0.0	29.4 <sup>+</sup>	69.5	44.2	1.57
	A3	30.6	200	120	167	1.92	0.32	416	275	150	2	0.0	27.9 <sup>+</sup>	63.1	45.9	1.37
	B3	29.7	200	120	167	1.92	0.32	416	275	150	2	0.0	34.9 <sup>+</sup>	61.1	44.0	1.39
	C3	28.4	200	120	167	1.92	0.32	416	275	150	2	0.0	18.4 <sup>+</sup>	60.2	46.3	1.30
	A4	30.6	200	120	167	1.92	0.32	416	275	150	1	0.0	24.0 <sup>+</sup>	118.7	99.7	1.19
	B4	29.7	200	120	167	1.92	0.32	416	275	150	1	0.0	29.4 <sup>+</sup>	131.3	97.7	1.34
	C4	28.4	200	120	167	1.92	0.32	416	275	150	1	0.0	18.3 <sup>+</sup>	146.8	95.8	1.53
A5	30.6	200	120	167	1.92	0.32	416	275	150	2	0.0	23.6 <sup>+</sup>	50.2	46.8	1.07	
B5	29.7	200	120	167	1.92	0.32	416	275	150	2	0.0	34.1 <sup>+</sup>	47.7	44.1	1.08	
C5	28.4	200	120	167	1.92	0.32	416	275	150	2	0.0	19.4 <sup>+</sup>	67.3	46.1	1.46	

(continued on next page)

(continued)

Reference	Specimen	$f_{cyl,150}$ (MPa)	$h$ (mm)	$b_w$ (mm)	$d$ (mm)	$\rho_l$ (%)	$\rho_v$ (%)	$f_f$ (MPa)	$f_{fv}$ (MPa)	$s$ (mm)	$a/d$	$\eta_{l,sn}$ (%)	$\eta_{w,sn}$ (%)	$V_{test}$ (kN)	$V_{pred,CCCM}$ (kN)	$V_{test}/V_{pred}$	
Higgins and Farrow (2006) [58]	A6	30.6	200	120	167	1.92	0.32	416	275	150	1	0.0	24.6 <sup>+</sup>	124.5	99.7	1.25	
	B6	29.7	200	120	167	1.92	0.32	416	275	150	1	0.0	26.1 <sup>+</sup>	117.9	97.9	1.20	
	C6	28.4	200	120	167	1.92	0.32	416	275	150	1	0.0	22.7 <sup>+</sup>	129.3	95.6	1.35	
	8RA	29.3	610	254	521	1.9	0.49	441	496	203	2.04	0.0	0.0	594	549.4	1.08	
	8RD	29.3	610	254	521	1.9	0.49	441	496	203	2.04	0.0	0.0	471	410.2	1.15	
	10RA	33.4	610	254	521	1.9	0.39	441	496	254	2.04	0.0	0.0	578	485.7	1.19	
	10RB	33.4	610	254	521	1.9	0.39	441	496	254	2.04	0.0	13.2	507	422.4	1.20	
	10RC	33.4	610	254	521	1.9	0.39	441	496	254	2.04	0.0	23.1	467	392.7	1.19	
	10RD	33.4	610	254	521	1.9	0.39	441	496	254	2.04	0.0	26.0	405	383.9	1.05	
	12RA	29.6	610	254	521	1.9	0.33	441	496	305	2.04	0.0	0.0	489	424.4	1.15	
	12RD	29.6	610	254	521	1.9	0.33	441	496	305	2.04	0.0	33.8	443	321.1	1.38	
	Li and Yin (2010) [59]	BW-0	27.0	200	150	166	2.30	0.25	210	275	150	2.0	0.0	0.0	88.0	64.7	1.36
BW-1		27.0	200	150	166	2.30	0.25	210	275	150	2.0	1.0 <sup>+</sup>	0.8 <sup>+</sup>	83.0	64.5	1.29	
BW-2		27.0	200	150	166	2.30	0.25	210	275	150	2.0	1.6 <sup>+</sup>	1.8 <sup>+</sup>	77.8	64.2	1.21	
BW-3		27.0	200	150	166	2.30	0.25	210	275	150	2.0	2.6 <sup>+</sup>	1.9 <sup>+</sup>	75.9	64.1	1.18	
BSP-1A		27.0	200	150	166	2.30	0.25	210	275	150	1.5	2.6 <sup>+</sup>	1.9 <sup>+</sup>	126.0	89.1	1.41	
BSP-1B		27.0	200	150	166	2.30	0.25	210	275	150	1.5	2.9 <sup>+</sup>	2.0 <sup>+</sup>	131.0	89.0	1.47	
BSP-2A		27.0	200	150	166	2.30	0.25	210	275	150	1.8	2.7 <sup>+</sup>	2.0 <sup>+</sup>	106.5	71.3	1.49	
BSP-2B		27.0	200	150	166	2.30	0.25	210	275	150	1.8	2.9 <sup>+</sup>	2.0 <sup>+</sup>	96.0	71.3	1.35	
BSP-3A		27.0	200	150	166	2.30	0.25	210	275	150	2.2	2.5 <sup>+</sup>	1.9 <sup>+</sup>	82.5	59.9	1.38	
BSP-3B		27.0	200	150	166	2.30	0.25	210	275	150	2.2	2.5 <sup>+</sup>	2.0 <sup>+</sup>	79.0	59.9	1.32	
Juarez et al (2011) [60]		V71-150	21.0	350	200	300	0.99	0.30	420	420	150	2	0.0	0.0	115	159.6	0.72
		V81-150	21.0	350	200	300	0.99	0.30	420	420	150	2	0.0	0.0	120	159.6	0.75
	V3M-150	21.0	350	200	300	0.99	0.30	420	420	150	2	0.0	34.0	68	118.3	0.57	
	V4M-150	21.0	350	200	300	0.99	0.30	420	420	150	2	0.0	52.7	91	100.1	0.91	
	V5S-150	21.0	350	200	300	0.99	0.30	420	420	150	2	0.0	68.4	80	84.9	0.94	
	V6S-150	21.0	350	200	300	0.99	0.30	420	420	150	2	0.0	60.9	86	92.1	0.93	
	V131-200	21.0	350	200	300	0.99	0.23	420	420	200	2	0.0	0.0	120	134.6	0.89	
	V141-200	21.0	350	200	300	0.99	0.23	420	420	200	2	0.0	0.0	98	134.6	0.73	
	V11M-200	21.0	350	200	300	0.99	0.23	420	420	200	2	0.0	43.8	77	96.8	0.80	
	V12M-200	21.0	350	200	300	0.99	0.23	420	420	200	2	0.0	34.0	87	104.0	0.84	
	V15S-200	21.0	350	200	300	0.99	0.23	420	420	200	2	0.0	68.4	80	78.7	1.02	
	V16S-200	21.0	350	200	300	0.99	0.23	420	420	200	2	0.0	68.4	89	78.7	1.13	
Zhao and Jin (2012) [61]	1-0	22.5	180	150	150	2.79	0.25	369	332	150	3.1	0.0	0.0	80	52.2	1.53	
	1-1	22.5	180	150	150	2.79	0.25	369	332	150	3.1	0.0	0.6	80	52.1	1.54	
	1-2	22.5	180	150	150	2.79	0.25	369	332	150	3.1	0.0	1.8	80	51.8	1.54	
	1-3	22.5	180	150	150	2.79	0.25	369	332	150	3.1	0.0	2.4	96	51.7	1.86	
	1-4	22.5	180	150	150	2.79	0.25	369	332	150	3.1	0.0	3.3	100	51.5	1.94	
	1-5	22.5	180	150	150	2.79	0.25	369	332	150	3.1	0.0	4.0	92	51.3	1.79	
	2-0	22.5	180	150	150	2.79	0.38	369	332	100	3.1	0.0	0.0	96	63.8	1.51	
	2-1	22.5	180	150	150	2.79	0.38	369	332	100	3.1	0.0	0.4	84	63.6	1.32	
	2-2	22.5	180	150	150	2.79	0.38	369	332	100	3.1	0.0	0.7	80	63.5	1.26	
	2-3	22.5	180	150	150	2.79	0.38	369	332	100	3.1	0.0	2.2	88	63.0	1.40	
	2-4	22.5	180	150	150	2.79	0.38	369	332	100	3.1	0.0	3.5	84	62.6	1.34	
	2-5	22.5	180	150	150	2.79	0.38	369	332	100	3.1	0.0	4.9	104	62.1	1.67	
	3-0	22.5	180	150	150	2.79	0.45	369	332	150	3.1	0.0	0.0	72	70.0	1.03	
	3-1	22.5	180	150	150	2.79	0.45	369	332	150	3.1	0.0	0.8	76	69.7	1.09	
	3-2	22.5	180	150	150	2.79	0.45	369	332	150	3.1	0.0	2.0	96	69.2	1.39	
	3-3	22.5	180	150	150	2.79	0.45	369	332	150	3.1	0.0	3.8	80	68.5	1.17	
	3-4	22.5	180	150	150	2.79	0.45	369	332	150	3.1	0.0	3.8	92	68.5	1.34	
	3-5	22.5	180	150	150	2.79	0.45	369	332	150	3.1	0.0	3.7	92	68.5	1.34	
	0	22.5	180	150	150	2.26	0.19	369	332	200	2.2	0.0	0.0	60	50.1	1.20	
	1	22.5	180	150	150	2.26	0.19	369	332	200	2.2	1.5	0.8	60	49.8	1.20	
2	22.5	180	150	150	2.26	0.19	369	332	200	2.2	2.8	1.7	65	49.6	1.31		
3	22.5	180	150	150	2.26	0.19	369	332	200	2.2	4.2	2.7	68	49.3	1.38		
4	22.5	180	150	150	2.26	0.19	369	332	200	2.2	6.6	4.0	69	48.9	1.41		
5	22.5	180	150	150	2.26	0.19	369	332	200	2.2	8.6	5.1	68	48.5	1.40		
6	22.5	180	150	150	2.26	0.19	369	332	200	2.2	11.6	6.3	72	48.1	1.50		
7	22.5	180	150	150	2.26	0.19	369	332	200	2.2	14.0	7.2	70	47.7	1.47		
8	22.5	180	150	150	2.26	0.19	369	332	200	2.2	19.0	8.3	67	47.1	1.42		
9	22.5	180	150	150	2.26	0.19	369	332	200	2.2	26.0	9.2	62	46.3	1.34		
Xue et al. (2013) [62]	B(1.5)-m1s	36.0	240	120	220	2.17	0.39	706	300	120	1.5	12.0	0.0	124.3	108.0	1.15	
	B(1.5)-m2s	37.0	240	120	220	2.17	0.39	706	300	120	1.5	16.6	0.0	115	107.9	1.07	
	B(2.0)-m1s	39.1	240	120	220	2.17	0.39	706	300	120	2	15.1	0.0	89.3	88.3	1.01	
		39.3	240	120	220	2.17	0.39	706	300	120	2	15.0	0.0	103.1	88.5	1.17	

(continued on next page)

(continued)

Reference	Specimen	$f_{cyl,150}$ (MPa)	$h$ (mm)	$b_w$ (mm)	$d$ (mm)	$\rho_l$ (%)	$\rho_v$ (%)	$f_y$ (MPa)	$f_{yv}$ (MPa)	$s$ (mm)	$a/d$	$\eta_{l,sn}$ (%)	$\eta_{w,sn}$ (%)	$V_{test}$ (kN)	$V_{pred,CCCM}$ (kN)	$V_{test}/V_{pred}$	
	B(2.0)-m2s																
	B(2.6)-m1s	35.1	240	120	220	2.17	0.39	706	300	120	2.6	5.0	0.0	77.4	75.0	1.03	
	B(2.6)-m2s	35.9	240	120	220	2.17	0.39	706	300	120	2.6	32.0	0.0	82.1	70.7	1.16	
	B(3.2)-m1s	34.9	240	120	220	2.17	0.39	706	300	120	3.2	8.0	0.0	70.5	72.8	0.97	
	B(3.2)-m2s	33.3	240	120	220	2.17	0.39	706	300	120	3.2	8.5	0.0	71.7	71.8	1.00	
Xue et al. (2014) [63]	B (39)-s0	33.1	240	120	220	2.17	0.39	706	300	120	2.6	0.0	0.0	74.0	74.4	1.00	
	B (39)-s1	34.2	240	120	220	2.17	0.39	706	300	120	2.6	0.8	6.1	72.0	72.7	0.99	
	B (39)-s2	33.9	240	120	220	2.17	0.39	706	300	120	2.6	1.0	11.2	74.1	64.2	1.15	
	B (39)-s3	34.6	240	120	220	2.17	0.39	706	300	120	2.6	1.6	20.9	69.5	61.0	1.14	
	B (39)-s4	35.1	240	120	220	2.17	0.39	706	300	120	2.6	1.8	27.6	70.4	58.8	1.20	
	B (39)-s5	34.9	240	120	220	2.17	0.39	706	300	120	2.6	0.9	34.2	69.5	56.3	1.23	
	B (52)-s0	33.1	240	120	220	2.17	0.52	706	300	90	2.6	0.0	0.0	84.1	86.6	0.97	
	B (52)-s1	34.9	240	120	220	2.17	0.52	706	300	90	2.6	0.8	9.0	87.9	83.2	1.06	
	B (52)-s2	34.6	240	120	220	2.17	0.52	706	300	90	2.6	0.7	15.0	80.7	72.3	1.12	
	B (52)-s3	33.9	240	120	220	2.17	0.52	706	300	90	2.6	0.7	22.0	72.1	68.6	1.05	
El-Sayed et al. (2016) [64]	B10-200	34.9	350	200	325	3.27	0.25	480	495	200	3	0.0	9.8 <sup>+</sup>	157	182.7	0.86	
	B20-200	40.7	350	200	325	3.27	0.25	480	495	200	3	0.0	23.1 <sup>+</sup>	136	168.0	0.81	
	B10-150	34.6	350	200	325	3.27	0.34	480	495	150	3	0.0	14.0 <sup>+</sup>	166	193.5	0.86	
	B20-150	40.9	350	200	325	3.27	0.34	480	495	150	3	0.0	22.8 <sup>+</sup>	173	190.4	0.91	
	B10-100	44.4	350	200	325	3.27	0.50	480	495	100	3	0.0	12.2 <sup>+</sup>	204	260.2	0.78	
	B20-100	44.0	350	200	325	3.27	0.50	480	495	100	3	0.0	24.5 <sup>+</sup>	172.5	236.3	0.73	
Imam and Azad (2016) [65]	A1-10	33.1	220	140	170	1.48	0.90	580	560	80	1.76	0.0	38.8 <sup>+</sup>	96.1	72.5	1.32	
	A2-10	33.1	220	140	170	1.48	0.90	580	560	80	1.76	0.0	41.1 <sup>+</sup>	81.6	75.2	1.08	
	A3-10	33.1	220	140	170	1.48	0.90	580	560	80	1.76	0.0	52.7 <sup>+</sup>	83.5	66.6	1.25	
	A4-6	33.1	220	140	170	1.48	0.90	580	560	80	1.76	0.0	28.5 <sup>+</sup>	88.5	74.1	1.19	
	A5-6	33.1	220	140	170	1.48	0.90	580	560	80	1.76	0.0	30.5 <sup>+</sup>	87.6	74.1	1.18	
	A6-6	33.1	220	140	170	1.48	0.90	580	560	80	1.76	0.0	26.4 <sup>+</sup>	90	74.1	1.21	
	A7-6	33.1	220	140	170	1.48	0.90	580	560	80	1.76	0.0	28.6 <sup>+</sup>	103	74.1	1.39	
	B1-10	33.1	240	150	190	1.22	0.84	580	560	80	1.57	0.0	40.0 <sup>+</sup>	80.9	90.0	0.90	
	B2-10	33.1	240	150	190	1.22	0.84	580	560	80	1.57	0.0	36.4 <sup>+</sup>	103	92.8	1.11	
	B3-10	33.1	240	150	190	1.22	0.84	580	560	80	1.57	0.0	31.3 <sup>+</sup>	105	96.9	1.08	
	B4-10	33.1	240	150	190	1.22	0.84	580	560	80	1.57	0.0	39.6 <sup>+</sup>	90	90.4	1.00	
	B5-6	33.1	240	150	190	1.22	0.84	580	560	80	1.57	0.0	22.8 <sup>+</sup>	119.1	97.0	1.23	
	B6-6	33.1	240	150	190	1.22	0.84	580	560	80	1.57	0.0	23.4 <sup>+</sup>	110	97.0	1.13	
Lu et al. (2019) [57]	A-1	40.8	300	200	259	2.20	0.14	390	339	150	2.00	14.4	54.2	147.7	101.3	1.46	
	A-2	40.8	300	200	259	2.20	0.10	390	339	200	2.5	1.8	7.6	137.8	99.6	1.38	
	A-3	40.8	300	200	259	2.20	0.16	390	373	250	3.0	16.5	46.5	119.8	87.2	1.37	
	A-4	40.8	300	200	259	2.20	0.20	390	373	200	3.5	15.6	44.3	109.8	90.0	1.22	
	A-5	40.8	300	200	259	2.20	0.15	390	458	150	2.00	15.5	55.6	151.6	106.3	1.43	
	A-6	40.8	300	200	259	2.20	0.11	390	458	200	2.5	0.0	0.0	139.2	111.8	1.25	
	A-7	40.8	300	200	259	2.20	0.16	390	433	250	3.0	22.7	60.1	115.4	83.4	1.38	
	A-9	40.8	300	200	259	2.20	0.14	390	476	150	2.00	9.9	38.2	181.5	115.0	1.58	
	A-10	40.8	300	200	259	2.20	0.11	390	476	200	2.5	4.3	17.6	111.8	98.6	1.13	
	A-11	40.8	300	200	259	2.20	0.14	390	524	250	3.0	12.7	38.7	93.8	96.9	0.97	
	A-12	40.8	300	200	259	2.20	0.18	390	524	200	3.5	13.5	40.8	121.3	99.1	1.22	
	B-1	50.0	300	200	259	2.20	0.14	390	339	150	2.00	0.0	0.0	145.4	145.7	1.00	
	B-2	50.0	300	200	259	2.20	0.10	390	339	200	2.5	3.2	13.3	119.8	100.4	1.19	
	B-3	50.0	300	200	259	2.20	0.16	390	373	250	3.0	10.4	30.5	125.7	103.0	1.22	
	B-5	50.0	300	200	259	2.20	0.15	390	458	150	2.00	10.4	39.4	179.6	125.6	1.43	
	B-6	50.0	300	200	259	2.20	0.11	390	458	200	2.5	14.1	51.4	133.5	93.5	1.43	
	B-7	50.0	300	200	259	2.20	0.16	390	433	250	3.0	15.8	44.1	115.8	100.6	1.15	
	B-9	50.0	300	200	259	2.20	0.14	390	476	150	2.00	13.7	51.1	129.2	119.5	1.08	
	B-10	50.0	300	200	259	2.20	0.11	390	476	200	2.5	10.6	40.7	155.8	98.0	1.59	
	B-11	50.0	300	200	259	2.20	0.14	390	524	250	3.0	10.5	32.4	109.8	108.7	1.01	
																<b>Number</b>	
																	<b>Mean</b>
																	<b>1.19</b>
																	<b>(1.20)</b>
																	<b>Std. dev,</b>
																	<b>0.24</b>
																	<b>(0.23)</b>
																	<b>COV</b>
																	<b>19.95</b>
																	<b>(19.35)</b>
																	<b>MIN</b>
																	<b>0.57</b>
																	<b>(0.57)</b>
																	<b>MAX</b>
																	<b>1.94</b>
																	<b>(1.94)</b>
																	<b>5%</b>
																	<b>0.80</b>
																	<b>(0.82)</b>
																	<b>95%</b>
																	<b>1.54</b>
																	<b>(1.54)</b>

\* Beams tested by Rodriguez et al. (1997) suffered high corrosion levels, including the top compressive reinforcement. As commented in Section 5.3 (Fig. 9d), the reduction of the effective depth, due to concrete spalling of the concrete above the stirrups was exceptionally considered in this case (10 beams). The  $V_{test}/V_{pred}$  values calculated considering this reduction are given in brackets.

† Values of  $\eta_{l,sn}$  or  $\eta_{w,sn}$  marked with this sign (+) have been computed using Eq. (22), as they were original reported with weight loss ratio.

## References

- [1] Fernandez I, Bairán JM, Marí AR. Corrosion effects on the mechanical properties of reinforcing steel bars. Fatigue and  $\sigma$ - $\epsilon$  behavior. *Constr Build Mater* 2015;101:772–83. <https://doi.org/10.1016/j.conbuildmat.2015.10.139>.
- [2] Al-Sulaimani GJ, Kaleemullah M, Basunbul IA, Rasheeduzzafar. Influence of corrosion and cracking on bond behavior and strength of reinforced concrete members. *ACI Struct J* 1990;87:220–31. <https://doi.org/10.14359/2732>.
- [3] Alonso C, Andrade C, Rodriguez J, Diez JM. Factors controlling cracking of concrete affected by reinforcement corrosion. *Mater Struct Constr* 1998;31(7):435–41. <https://doi.org/10.1007/BF02480466>.
- [4] Broomfield JP. *Corrosion of Steel in Concrete: Understanding, Investigation and Repair*. 2nd ed. Abingdon; 2006.
- [5] Schmitt G, Schütze M, Hays GF, Burns W, Han EH, Pourbaix A, et al. *Global Needs for Knowledge Dissemination, Research, and Development in Materials Deterioration and Corrosion Control*. 2009.
- [6] Stewart Mark G, Wang Xiaoming, Nguyen Minh N. Climate change impact and risks of concrete infrastructure deterioration. *Eng Struct* 2011;33(4):1326–37. <https://doi.org/10.1016/j.engstruct.2011.01.010>.
- [7] Bastidas-Arteaga E, Stewart MG. Damage risks and economic assessment of climate adaptation strategies for design of new concrete structures subject to chloride-induced corrosion. *Struct Saf* 2015;52:40–53. <https://doi.org/10.1016/j.strusafe.2014.10.005>.
- [8] Rózsás Á, Kovács N, Vigh LG, Sýkora M. Climate change effects on structural reliability in the Carpathian Region. *Q J Hungarian Meteorol Serv n.d.*;120:103–25.
- [9] Andrade C. Some historical notes on the research in corrosion of reinforcement. *Hormigón y Acero* 2018;69:21–8. <https://doi.org/10.1016/j.hya.2018.12.002>.
- [10] Muñoz Noval A. Comportamiento de vigas hiperestáticas de hormigón armado corroídas y reparadas con mortero. Pérdida de propiedades mecánicas del acero de refuerzo y fisuración del recubrimiento de hormigón por corrosión. E.T.S.I. Caminos, Canales y Puertos (UPM); 2009.
- [11] Fernandez Ignasi, Herrador Manuel F, Marí Antonio R, Bairán Jesús Miguel. Structural effects of steel reinforcement corrosion on statically indeterminate reinforced concrete members. *Mater Struct Constr* 2016;49(12):4959–73. <https://doi.org/10.1617/s11527-016-0836-2>.
- [12] Fernandez I, Herrador MF, Marí AR, Bairán JM. Ultimate Capacity of Corroded Statically Indeterminate Reinforced Concrete Members. *Int J Concr Struct Mater* 2018;12:1–23. <https://doi.org/10.1186/s40069-018-0297-9>.
- [13] Bossio A, Fabbrocino F, Monetta T, Lignola GP, Prota A, Manfredi G, et al. Corrosion effects on seismic capacity of reinforced concrete structures. *Corros Rev* 2019;37:45–56. <https://doi.org/10.1515/correv-2018-0044>.
- [14] Recupero A, Spinella N, Tondolo F. Failure analysis of corroded RC beams subjected to shear-flexural actions. *Eng Fail Anal* 2018;93:26–37. <https://doi.org/10.1016/j.engfailanal.2018.06.025>.
- [15] Capacci Luca, Biondini Fabio. Probabilistic life-cycle seismic resilience assessment of aging bridge networks considering infrastructure upgrading. *Struct Infrastruct Eng* 2020;16(4):659–75. <https://doi.org/10.1080/15732479.2020.1716258>.
- [16] Meet Sompura, Trishna Choudhury, Naveen Kwatra. Investigating the nonlinear performance of corroded reinforced concrete beams. *J Build Eng* 2021;44:102640. <https://doi.org/10.1016/j.jobbe.2021.102640>.
- [17] Bojórquez Juan, Ponce Sandra, Ruiz Sonia E, Bojórquez Edén, Reyes-Salazar Alfredo, Barraza Manuel, et al. Structural reliability of reinforced concrete buildings under earthquakes and corrosion effects. *Eng Struct* 2021;237:112161. <https://doi.org/10.1016/j.engstruct.2021.112161>.
- [18] Biondini Fabio, Vergani Matteo. Deteriorating beam finite element for nonlinear analysis of concrete structures under corrosion. *Struct Infrastruct Eng* 2015;11(4):519–32. <https://doi.org/10.1080/15732479.2014.951863>.
- [19] Marí A, Bairán J, Oller E, Fernandez I. Numerical simulation of the structural effects of the deterioration in concrete structures. *Proc. fib Symp. "Concrete Struct. Sustain. Community"*. 2012.
- [20] Marí A, Bairán J, Oller E, Duarte N. Modeling serviceability performance and ultimate capacity of corroded reinforced and prestressed concrete structures. *Struct Concr* 2021. <https://doi.org/10.1002/suco.202100159>.
- [21] Poliotti M, Bairán JM. A new concrete plastic-damage model with an evolutive dilatancy parameter. *Eng Struct* 2019;189:541–9. <https://doi.org/10.1016/j.engstruct.2019.03.086>.
- [22] CEN. *Eurocode 2: Design of Concrete Structures: Part 1: General Rules and Rules for Buildings*. European Committee for Standardization; 2002.
- [23] ACI Committee 318. *Building Code Requirements for Structural Concrete and Commentary (ACI 318-19)*; 2019. <http://dx.doi.org/10.14359/51716937>.
- [24] Mancini G, Carbone VI, Gino D. From experiments to design: A probabilistic definition of design formulations from empirical and semi-empirical resistance models. *Hormigón y Acero* 2018;69:29–34. <https://doi.org/10.1016/j.hya.2017.12.003>.
- [25] Vecchio FJ, Collins MP. The modified compression-field theory for reinforced concrete elements subjected to shear. *ACI Struct J* 1986;83:219–31. <https://doi.org/10.14359/10416>.
- [26] Muttoni A, Fernandez-Ruiz M. Shear Strength of Members without Transverse Reinforcement as Function of Critical Shear Crack Width. *ACI Struct J* 2008;105:163–72.
- [27] Zararis Prodromos D, Papadakis George Ch. Diagonal shear failure and size effect in RC beams without web reinforcement. *J Struct Eng* 2001;127(7):733–42. [https://doi.org/10.1061/\(ASCE\)0733-9445\(2001\)127:7\(733\)](https://doi.org/10.1061/(ASCE)0733-9445(2001)127:7(733)).
- [28] Park HG, Kang S, Choi KK. Analytical model for shear strength of ordinary and prestressed concrete beams. *Eng Struct* 2013;46:94–103. <https://doi.org/10.1016/j.engstruct.2012.07.015>.
- [29] Tureyen AK, Frosch RJ. *Concrete Shear Strength: Another Perspective*. *ACI Struct J* 2003;100:609–15.
- [30] Cladera A, Marí A, Bairán JM, Ribas C, Oller E, Duarte N. The compression chord capacity model for the shear design and assessment of reinforced and prestressed concrete beams. *Struct Concr* 2016;17:1017–32. <https://doi.org/10.1002/suco.201500214>.
- [31] Marí Antonio, Bairán Jesús, Cladera Antoni, Oller Eva, Ribas Carlos. Shear-flexural strength mechanical model for the design and assessment of reinforced concrete beams. *Struct Infrastruct Eng* 2015;11(11):1399–419. <https://doi.org/10.1080/15732479.2014.964735>.
- [32] Bairán JM, Mendiña R, Marí A, Cladera A. Shear strength of non-slender reinforced concrete beams. *ACI Struct J* 2020;117:277–89. <https://doi.org/10.14359/51721369>.
- [33] Cladera A, Ribas C, Oller E, Marí A. Shear fatigue strength of reinforced concrete members without transverse reinforcement according to the compression chord capacity model. *Eng Struct* 2020;211. <https://doi.org/10.1016/j.engstruct.2020.110495>.
- [34] Marí A, Spinella N, Recupero A, Cladera A. Mechanical model for the shear strength of steel fiber reinforced concrete (SFRC) beams without stirrups. *Mater Struct Constr* 2020;53. <https://doi.org/10.1617/s11527-020-01461-4>.
- [35] Marí A, Cladera A, Ribas C, Oller E, Bairán J. Simplified Multi-Action Shear Model for Plain or Steel Fibre Reinforced Concrete Beams Longitudinally Reinforced with Steel or FRP Bars. *Towar. a Ration. Underst. Shear beams slabs - fib Bull.* 2018;85:260–73.
- [36] Rius JM, Cladera A, Ribas C, Mas B. Shear strengthening of reinforced concrete beams using shape memory alloys. *Constr Build Mater* 2019;200:420–35. <https://doi.org/10.1016/j.conbuildmat.2018.12.104>.
- [37] Montoya-Coronado Luis A, Ruiz-Pinilla Joaquín G, Ribas Carlos, Cladera Antoni. Experimental study on shear strengthening of shear critical RC beams using iron-based shape memory alloy strips. *Eng Struct* 2019;200:109680. <https://doi.org/10.1016/j.engstruct.2019.109680>.
- [38] Rodriguez J, Ortega LM, Casal J. Load carrying capacity of concrete structures with corroded reinforcement. *Constr Build Mater* 1997;11(4):239–48. [https://doi.org/10.1016/S0950-0618\(97\)00043-3](https://doi.org/10.1016/S0950-0618(97)00043-3).
- [39] Coronelli D, Gambarova P. Structural Assessment of Corroded Reinforced Concrete Beams: Modeling Guidelines. *J Struct Eng* 2004;130(8):1214–24. [https://doi.org/10.1061/\(ASCE\)0733-9445\(2004\)130:8\(1214\)](https://doi.org/10.1061/(ASCE)0733-9445(2004)130:8(1214)).
- [40] Higgins C, Farrow WC, Potisuk T, Miller TH, Yim SC, Holcomb GR, et al. *Shear Capacity Assessment of Corrosion-Damaged Reinforced Concrete Beams*; 2003.
- [41] EC Innovation Programme IN30902I. CONTECVET: A validated Users Manual for assessing the residual service life of concrete structures; 2001. Available at: [https://www.ietcc.csic.es/wp-content/uploads/1989/02/manual\\_contecvet\\_ingles.pdf](https://www.ietcc.csic.es/wp-content/uploads/1989/02/manual_contecvet_ingles.pdf).
- [42] Lin Hongwei, Zhao Yuxi, Feng Peng, Ye Hailong, Ozbolt Josko, Jiang Cheng, et al. State-of-the-art review on the bond properties of corroded reinforcing steel bar. *Constr Build Mater* 2019;213:216–33. <https://doi.org/10.1016/j.conbuildmat.2019.04.077>.
- [43] Kupfer Helmut B, Gerstle Kurt H. Behavior of concrete under biaxial stresses. *J Eng Mech Div* 1973;99(4):853–66.
- [44] Bairán Jesús Miguel, Marí Antonio, Cladera Antoni. Analysis of shear resisting actions by means of optimization of strut and tie models taking into account crack patterns. *Hormigón y Acero* 2018;69(286):197–206. <https://doi.org/10.1016/j.hya.2017.04.009>.
- [45] Cladera A, Marí A, Bairán J-M, Oller E, Ribas C. One-Way Shear Design Method Based on a Multi-Action Model. *Concr Int* 2017;39:40–6.
- [46] Carmona Jacinto R, Ruiz Gonzalo, del Viso Javier R. Mixed-mode crack propagation through reinforced concrete. *Eng Fract Mech* 2007;74(17):2788–809. <https://doi.org/10.1016/j.engfracmech.2007.01.004>.
- [47] Bazant ZP, Yu Q, Gerstle W, Hanson J, Ju JW. Justification of ACI 446 Proposal for Updating ACI Code Provisions for Shear Design of Reinforced Concrete Beams. *Struct J* 2007;104:601–10.
- [48] Reineck K-H, Bentz EC, Fitik B, Kuchma DA, Bayrak O. ACI-DAFStb database of shear tests on slender reinforced concrete beams without stirrups. *ACI Struct J* 2013;110:867–75.
- [49] Reineck K-H, Bentz E, Fitik B, Kuchma DA, Bayrak O. ACI-DAFStb Databases for Shear Tests on Slender Reinforced Concrete Beams with Stirrups. *ACI Struct J* 2014;111:1147–56.
- [50] Schlaich Jorg, Schafer Kurt, Jennewein Mattias. Toward a Consistent Design of Structural Concrete. *PCI J* 1987;32(3):74–150.
- [51] Vollum RL, Fang L. Shear enhancement in RC beams with multiple point loads. *Eng Struct* 2014;80:389–405. <https://doi.org/10.1016/j.engstruct.2014.09.010>.
- [52] Reineck KH, Todisco L. Database of shear tests for non-slender reinforced concrete beams without stirrups. *ACI Struct J* 2014;111:1363–71. <https://doi.org/10.14359/51686820>.
- [53] Todisco L, Reineck K-H, Bayrak O. Database with Shear Tests on Non-Slender Reinforced Concrete Beams with Vertical Stirrups. *Struct J* 2015;112:761–9.
- [54] Lu ZH, Li H, Li W, Zhao YG, Dong W. An empirical model for the shear strength of corroded reinforced concrete beam. *Constr Build Mater* 2018;188:1234–48. <https://doi.org/10.1016/j.conbuildmat.2018.08.123>.
- [55] Soltani Mahmoodreza, Abu-Abailah Adham, Scott Rowe Bryan. Statistical Approach to Modeling Reduced Shear Capacity of Corrosion-Damaged Reinforced Concrete Beams. *Pract Period Struct Des Constr* 2021;26(2):04020073. [https://doi.org/10.1061/\(ASCE\)JSC.1943-5576.0000564](https://doi.org/10.1061/(ASCE)JSC.1943-5576.0000564).

- [56] Xu SH, Niu DT. The shear behavior of corroded simply supported reinforced concrete beam (in Chinese). *J Build Struct* 2004;25:98–104.
- [57] Lu Zhao-Hui, Li Hai, Li Wengui, Zhao Yan-Gang, Tang Zhuo, Sun Zhihui. Shear behavior degradation and failure pattern of reinforced concrete beam with chloride-induced stirrup corrosion. *Adv Struct Eng* 2019;22(14):2998–3010. <https://doi.org/10.1177/1369433219855917>.
- [58] Higgins C, Farrow WC. Tests of reinforced concrete beams with corrosion-damaged stirrups. *ACI Struct J* 2006;103:133–41. <https://doi.org/10.14359/15094>.
- [59] Li XT, Yin HG. Degradation Mechanism and Predicting Models of Shearing Capacity for Corroded Reinforced Concrete Beams (in Chinese). *J Xuzhou Inst Technol (Natural Sci Ed)* 2010;25:58–63.
- [60] Juarez CA, Guevara B, Fajardo G, Castro-Borges P. Ultimate and nominal shear strength in reinforced concrete beams deteriorated by corrosion. *Eng Struct* 2011;33(12):3189–96. <https://doi.org/10.1016/j.engstruct.2011.08.014>.
- [61] Zhao YX, Jin WL. Analysis on shearing capacity of concrete beams with corroded stirrups (in Chinese). *J Zhejiang Univ (Eng Sci)* 2012;8:19–24.
- [62] Xue X, Seki H, Chen ZW. Shear capacity of RC beams containing corroded longitudinal bars. In Proc. Thirteenth. East Asia-Pacific Conf. Struct. Eng. Constr., Sapporo, Japan: The Thirteenth East Asia-Pacific Conference on Structural Engineering and Construction (EASEC-13); 2013, p. C-6–2.
- [63] Xue X, Seki H, Song Y. Shear Behavior of RC Beams Containing Corroded Stirrups. *Adv Struct Eng* 2014;17(2):165–77. <https://doi.org/10.1260/1369-4332.17.2.165>.
- [64] El-Sayed AK, Hussain RR, Shuraim AB. Influence of Stirrup Corrosion on Shear Strength of Reinforced Concrete Slender Beams. *ACI Struct J* 2016;113:1223–32. <https://doi.org/10.14359/51689147>.
- [65] Imam Ashhad, Azad Abul Kalam. Prediction of residual shear strength of corroded reinforced concrete beams. *Int J Adv Struct Eng* 2016;8(3):307–18. <https://doi.org/10.1007/s40091-016-0133-x>.
- [66] Comisión Permanente del Hormigón. Instrucción de Hormigón Estructural EHE-2008. Madrid: Ministerio de Fomento; 2008.
- [67] Fu Bo, Feng De-Cheng. A machine learning-based time-dependent shear strength model for corroded reinforced concrete beams. *J Build Eng* 2021;36:102118. <https://doi.org/10.1016/j.job.2020.102118>.